

## Natural Convection in Porous Enclosure caused by Partial Heating or Cooling

Watit Pakdee\*, Phadungsak Rattanadecho

Research Center of Microwave Utilization in Engineering (RCME)  
Department of Mechanical Engineering, Faculty of Engineering,  
Thammasat University, Rangsit Campus,  
Klong Luang, Pathumtani 12120, Thailand  
Tel: 0-2564-3001-5, Fax: 0-2564-3010, \*E-mail: [pwatit@engr.tu.ac.th](mailto:pwatit@engr.tu.ac.th)

### Abstract

Numerical studies of transient natural convection flow through a fluid-saturated porous medium in a square enclosure with a convection surface condition were conducted. Physical problem consists of a rectangular cavity filled with porous medium. The cavity is insulated except the top wall that is partially exposed to an outside ambient. The exposed surface allows convective transport through the porous medium, generating a thermal stratification and flow circulations. The formulation of differential equations is nondimensionalized and then solved numerically under appropriate initial and boundary conditions using the finite difference method. The finite difference equations handling the convection boundary condition of the open top surface are derived for heating and cooling conditions. A lateral temperature gradient in the region close to the top wall induces the buoyancy force under an unstable condition. The two-dimensional flow is characterized mainly by two symmetrical vortices driven by the effect of buoyancy. The directions of vortex rotation generated under the two different conditions are opposite. Unsteady effects of associated parameters were examined. It was found that the heat transfer coefficient, Rayleigh number and Darcy number considerably influenced characteristics of flow and heat transfer mechanisms. Furthermore, the flow pattern is found to have a local effect on the heat convection rate.

**Keywords:** natural convection, saturated porous media, convection boundary condition, partial cooling, partial heating

### 1. Introduction

It has been found that the fluid flows in cavity that experiences convective heating or cooling at the surface are involved in a wide variety of applications including lakes and geothermal reservoirs, underground water flow, solar collector etc. [1]. Associated industrial applications include secondary and tertiary oil recovery, growth of crystals [2], heating and drying process [3-5], solidification of casting, sterilization etc. Natural or free convection in a porous medium has been studied extensively. Cheng [6] provides a comprehensive review

of the literature on free convection in fluid-saturated porous media with a focus on geothermal systems. Oosthuizen and Patrick [7] performed numerical studies of natural convection in an inclined square enclosure with part of one wall heated to a uniform temperature and with the opposite wall uniformly cooled to a lower temperature and with the remaining wall portions. The enclosure is partially filled with a fluid and partly filled with a porous medium, which is saturated with the same fluid. The main results considered were the mean heat transfer rate across the enclosure. Nithiarasu et al. [8] examined effects of variable porosity on convective flow patterns inside a porous cavity. The flow is triggered by sustaining a temperature gradient between isothermal lateral walls. The variation in porosity significantly affects natural flow convective pattern. Khanafer and Chamkha [9] performed numerical study of mixed convection flow in a lid-driven cavity filled with a fluid-saturated porous media. In this study, the influences of the Richardson number, Darcy number and the Rayleigh number play an important role on mixed convection flow inside a square cavity filled with a fluid-saturated porous media. Nithiarasu et al. [10] examined effects of applied heat transfer coefficient on the cold wall of the cavity upon flow and heat transfer inside a porous medium. The differences between the Darcy and non-Darcy flow regime are clearly investigated for different Darcy, Rayleigh and Biot numbers and aspect ratio. Variations in Darcy, Rayleigh and Biot numbers and aspect ratio significantly affect natural flow convective pattern. Recently, a numerical study was conducted by Bera and Khalili [11] on thermosolutal convection within a rectangular enclosure. It was found that anisotropy causes significant changes in Nusselt and Sherwood numbers. Bera et al. [12] considered double diffusive convection due to constant heating and cooling on the two vertical walls, based on a non-Darcy model inclined permeability tensor. Previous investigations have merely focused on momentum and energy transfer in cavity filled with a saturated porous medium subjected to prescribed temperature and prescribed wall heat flux conditions. However, only a very limited amount of numerical and

experimental work on momentum and energy transfer in a cavity filled with a saturated porous medium subjected to heat transfer coefficient boundary condition at the exposed portion of the top wall has been reported. The case, in which the top wall is partially exposed, is considered in our study for both heating and cooling aspect. The detailed parametric study was carried out for transient natural convective flow in a fluid-saturated porous medium filled in a square cavity. The top surface is partially open to the ambient, allowing the surface temperature to vary, depending on the influence of convection heat transfer mechanism. Computed results are depicted using temperature, flow distributions and heat transfer rates in terms of local and average Nusselt numbers. The influences of associated parameters such as heat transfer coefficient, Rayleigh number and Darcy number on the flow and thermal configurations were examined.

## 2. Problem Description

The computational domain, depicted in Figure 1 is a rectangular cavity of size  $W \times H$  filled with a fluid-saturated porous medium. Aspect ratio of unity ( $A=1$ ) is used in the present study. The domain boundary is insulated except the top wall, which is partially exposed to an ambient air. Using standard symbols, the initial and boundary conditions corresponding to the problem are of the following forms.

$$u = v = 0, T = T_i \text{ for } t = 0 \quad (1)$$

$$\left. \begin{aligned} u = v = 0 \text{ at } x = 0, W \quad 0 \leq y \leq H \\ u = v = 0 \text{ at } y = 0, H \quad 0 \leq x \leq W \end{aligned} \right\} \quad (2)$$

$$\left. \begin{aligned} \frac{\partial T}{\partial x} = 0 \text{ at } x = 0, W \quad 0 \leq y \leq H \\ \frac{\partial T}{\partial y} = 0 \text{ at } y = 0 \quad 0 \leq x \leq W \\ \frac{\partial T}{\partial y} = 0 \text{ at } y = H \quad 0 \leq x \leq L \text{ and } W-L \leq x \leq W \end{aligned} \right\} \quad (3)$$

The boundary condition at the exposed portion of the top wall is defined as

$$-k \frac{\partial T}{\partial y} = h[T_h - T_l] \text{ at } y = H \quad L \leq x \leq W - L, \quad (4)$$

where  $k$  and  $h$  are effective thermal conductivity and convection heat transfer coefficient.  $\varepsilon$  and  $\nu$  denotes porosity of porous medium and fluid viscosity, respectively. Subscript  $h$  and  $l$  represent respectively high and low temperature. This type of condition corresponds to the existence of convective heat transfer at the surface and is obtained from the surface energy balance.

The porous medium is assumed to be homogeneous and thermally isotropic and saturated with a fluid that is local thermodynamic equilibrium with the solid matrix. The fluid flow is unsteady, laminar and incompressible. The pressure work and viscous dissipation are all assumed negligible. The thermophysical properties of the

porous medium are taken to be constant. However, the Boussinesq approximation takes into account of the effect of density variation on the buoyancy force. Furthermore, the solid matrix is made of spherical particles, while the porosity and permeability of the medium are assumed to be uniform throughout the rectangular cavity. The governing equations describing the heat transfer phenomenon are given by

$$\frac{\partial u}{\partial x} + \frac{\partial v}{\partial y} = 0 \quad (5)$$

$$\frac{1}{\varepsilon} \frac{\partial u}{\partial t} + \frac{u}{\varepsilon^2} \frac{\partial u}{\partial x} + \frac{v}{\varepsilon^2} \frac{\partial u}{\partial y} = -\frac{1}{\rho_f} \frac{\partial P}{\partial x} + \frac{\nu}{\varepsilon} \left( \frac{\partial^2 u}{\partial x^2} + \frac{\partial^2 u}{\partial y^2} \right) - \frac{\mu u}{\rho_f \kappa} \quad (6)$$

$$\frac{1}{\varepsilon} \frac{\partial v}{\partial t} + \frac{u}{\varepsilon^2} \frac{\partial v}{\partial x} + \frac{v}{\varepsilon^2} \frac{\partial v}{\partial y} = -\frac{1}{\rho_f} \frac{\partial P}{\partial y} + \frac{\nu}{\varepsilon} \left( \frac{\partial^2 v}{\partial x^2} + \frac{\partial^2 v}{\partial y^2} \right) + g\beta(T - T_\infty) - \frac{\mu v}{\rho_f \kappa} \quad (7)$$

$$\sigma \frac{\partial T}{\partial t} + u \frac{\partial T}{\partial x} + v \frac{\partial T}{\partial y} = \alpha \left( \frac{\partial^2 T}{\partial x^2} + \frac{\partial^2 T}{\partial y^2} \right) \quad (8)$$

$$\sigma = \frac{[\varepsilon(\rho c_p)_f + (1 - \varepsilon)(\rho c_p)_s]}{(\rho c_p)_f}, \quad (9)$$

where  $\kappa$  is medium permeability,  $\beta$  is thermal expansion coefficient,  $\alpha$  is effective thermal diffusivity of the porous medium,  $\mu$  and  $\nu$  are viscosity and kinematic viscosity of the fluid respectively. In the present study, the heat capacity ratio  $\sigma$  is taken to be unity since the thermal properties of the solid matrix and the fluid are assumed identical. The momentum equation consists of the Brinkmann term, which accounts for viscous effects due to the presence of solid body [13]. This form of momentum equation is known as Brinkmann-extended Darcy model. Lauriat and Prasad [14] employed the Brinkmann-extended Darcy formulation to investigate the buoyancy effects on natural convection in a vertical enclosure. Although the viscous boundary layer in the porous medium is very thin for most engineering applications, inclusion of this term is essential for heat transfer calculations [11]. However, the inertial effect was neglected, as the flow was relatively low.

The variables are transformed into the dimensionless quantities defined as,

$$\left. \begin{aligned} X = \frac{x}{H}, Y = \frac{y}{H}, \tau = \frac{t\alpha}{H^2}, U = \frac{uH}{\alpha}, V = \frac{vH}{\alpha} \\ \zeta = \frac{\omega H^2}{\alpha}, \Psi = \frac{\psi}{\alpha}, \theta = \frac{T - T_l}{T_h - T_l} \end{aligned} \right\}, \quad (10)$$

where  $\omega$  and  $\psi$  represent dimensional vorticity and stream function, respectively. Symbol  $\alpha$  denotes thermal diffusivity. Temperatures  $T_l$  and  $T_h$  change their values according to the problem type. In the heating case,  $T_l$  is initial temperature of a medium, and  $T_h$  is an ambient

temperature. In the other case of cooling,  $T_h$  is set to be an initial temperature of the medium, while  $T_l$  is an ambient temperature instead. Thus the dimensionless form of the governing equations can be written as

$$\frac{\partial^2 \psi}{\partial X^2} + \frac{\partial^2 \psi}{\partial Y^2} = -\zeta \quad (11)$$

$$\varepsilon \frac{\partial \zeta}{\partial \tau} + U \frac{\partial \zeta}{\partial X} + V \frac{\partial \zeta}{\partial Y} = \varepsilon \text{Pr} \left( \frac{\partial^2 \zeta}{\partial X^2} + \frac{\partial^2 \zeta}{\partial Y^2} \right) + \varepsilon^2 \text{Ra} \text{Pr} \left( \frac{\partial \theta}{\partial X} \right) - \frac{\varepsilon^2 \text{Pr}}{\text{Da}} \zeta \quad (12)$$

$$\sigma \frac{\partial \theta}{\partial \tau} + U \frac{\partial \theta}{\partial X} + V \frac{\partial \theta}{\partial Y} = \alpha \left( \frac{\partial^2 \theta}{\partial X^2} + \frac{\partial^2 \theta}{\partial Y^2} \right), \quad (13)$$

where the Darcy number, Da is defined as  $\kappa/H^2$ , and  $\text{Pr} = \nu/\alpha$  is the Prandtl number. The Rayleigh number Ra, which gives the relative magnitude of buoyancy and viscous forces, is defined as  $\text{Ra} = g\beta(T_i - T_\infty)H^3/(\nu\alpha)$ .  $\text{Pr} = \nu/\alpha$  is the Prandtl number, where  $\alpha = k_e/(\rho c_p)_f$  is the thermal diffusivity.

### 3. Numerical Procedure

The thermal properties of the porous medium are taken to be constant. Specific heat ratio of unity is assumed. The effective thermal conductivity of the porous medium considered is 10 W/m·K.

In the present study, the iterative finite difference method is used to solve the transient dimensionless governing equations (Eqs. (10)-(12)) subject to their corresponding initial and boundary conditions given by the non-dimensional form of Eqs. (1)-(4). Approximation of convective terms is based on an upwind finite differencing scheme, which correctly represent the directional influence of a disturbance. A uniform grid resolution of  $61 \times 61$  was found to be sufficient for all smooth computations and computational time required in achieving steady-state conditions. Finer grids did not provide a noticeable change in the computed results. The finite difference form of boundary condition at the open part of the top surface is systematically derived, based on energy conservation principle. The boundary values of dimensionless temperature of a node  $i, j$   $\theta_{i,j}$  in the heating case are expressed as

$$\theta_{ij} = \frac{2\theta_{i-1,j} + \theta_{i-1,j} + \theta_{i+1,j} + 2\frac{h\Delta y}{k}}{2\left(\frac{h}{k}\Delta Y + 2\right)} \quad (14)$$

In the different case of cooling phenomenon, the expression is given by

$$\theta_{ij} = \frac{2\theta_{i-1,j} + \theta_{i-1,j} + \theta_{i+1,j}}{2\left(\frac{h}{k}\Delta Y + 2\right)} \quad (15)$$

It can be noticed that both the equations (14) and (15) are independent of an ambient temperature  $T_\infty$  as it has been eliminated during the derivation. Thus the solutions can be obtained regardless of a value of  $T_\infty$ .

In order to verify the accuracy of the present numerical study, the present numerical model was validated against the results obtained by Nithiarasu et al. [8] in the presence of porous medium, as shown in Figure 2. The values of  $\text{Ra} = 10^4$ ,  $\text{Da} = 0.01$  and  $\varepsilon = 0.6$  were chosen. Table 1 clearly shows a good agreement of the maximum values of the stream function and vertical velocity component between the present solution and that of Nithiarasu et al [8]. All of these favorable comparisons lend confidence in the accuracy of the present numerical model.

### 4. Results and Discussion

The following investigations were conducted for a range of controlling parameters, which are Darcy number (Da) Rayleigh number (Ra) and convective heat transfer coefficient (h). The porosity  $\varepsilon$  of 0.8 and unity aspect ratio ( $A=1$ ) were considered throughout in the present study. In order to assess global effects of these parameters, the streamlines and isotherm distributions inside the entire cavity are presented.

The heating condition was first investigated. The resulting computational fields were extracted at the time adequately long to ensure sufficient energy transferred throughout the domain. Figure 3 displays instantaneous images of the contour plots during the thermal and flow evolution. The Darcy number of 0.1,  $\text{Ra} = 5 \times 10^4$ ,  $\text{Pr} = 1.0$ ,  $h = 60 \text{ w/m}^2\text{K}$ , and  $\varepsilon = 0.8$  are considered. The two columns represent temperature and stream function. With the same contour levels, comparisons can be observed directly. The four snapshots from top to bottom in each column are results taken at the dimensionless times  $\tau = 0.013, 0.088, 0.168$ . The vertical temperature stratification is observed. The streamline contours exhibit circulation patterns, which are characterized by the two symmetrical vortices. The fluid flows as it is driven by the effect of buoyancy. This effect is distributed from the top wall of cavity where the fluid is heated through the partially open area. This indicates the non-uniform temperature at the top surface, leading to an unstable condition. Thus the buoyancy effect is associated with the lateral temperature gradient at locations near the top surface. Heated portions of the fluid become lighter than the rest of fluid, and are expanded laterally away from the center to the sides then flow down along the two vertical walls, leading to the clockwise and counter-clockwise flow circulations. These results suggest that the buoyancy forces are able to overcome the retarding influence of viscous forces. An increase in strength of the vortices develops fast during early simulation times, and its maximum magnitude reaches 0.25 at  $\tau = 0.1$ . After this time, the vortices are slowly weakened. Similarly, temperature distribution progressively evolves relatively fast in the early times. After the time  $\tau = 0.07$ , slow evolution is observed. This result corresponds to the decrease in strength of flow circulations. In the remaining area, the fluid is nearly stagnant suggesting that conduction is dominant due to minimal flow activities. This is because the viscous effects are large.

The convective cooling condition is imposed as for

the other simulation. All parameters are the same as those employed for the heating case. This aids in direct comparison. Figure 4 displays instantaneous images of the contour plots during the thermal and flow evolution. The four snapshots with the same contour levels from top to bottom in each column are results taken at the dimensionless times  $\tau = 0.013, 0.088, 0.168,$  and  $0.245$ . The vertical temperature stratification is observed. The streamline contours exhibit circulation patterns, which are characterized by the two symmetrical vortices. The fluid flows as it is driven by the effect of buoyancy. This effect is distributed from the top wall of cavity where the fluid is cooled through the partially open slot, causing lower temperature near the top boundary. The existence of the non-uniform temperature along the top surface, and a decrease of density in the direction of gravitational force lead to an unstable condition. Thus the buoyancy effect is associated with the lateral temperature gradients at locations near the top surface. High temperature portions of fluid become lighter than the lower temperature portions at the middle where the wall is open. These light portions from two sides then expand laterally towards the center, compressing the lower temperature portions, which are heavier. As a result, the downward flows along the vertical centerline are originated, while the lighter fluid will rise, cooling as it moves. Consequently, the circulation flow pattern is generated. The clockwise and counter-clockwise circulations are located respectively on the left side and right side within the enclosure. An increase in strength of the vortices develops fast during early simulation times, and its maximum magnitude reaches 6.0. Subsequently the vortices are weakened. Similarly, temperature distribution progressively evolves relatively fast in the early times. Slow evolution is observed after that. This result corresponds well with the decrease in strength of flow circulations.

In the case of heating configuration, effects of the Darcy number on the fluid flow and temperature inside the rectangular cavity are depicted in figure 5. The contour of isotherms and streamlines are plotted for different Darcy numbers while  $\mathcal{E}$ , Pr and h are kept at 0.8, 1.0 and  $60 \text{ w/m}^2\text{K}$  respectively. The Darcy number, which is directly proportional to the permeability of the porous medium, was set to 0.001 and 0.1. The case in which the porous medium is absent corresponds to infinite Darcy number. The presence of a porous medium within rectangular enclosure results in a force opposite to the flow direction which tends to resist the flow which corresponds to suppress in the thermal currents of the flow as compared to a medium with no porous (infinite Darcy number). It is evident that the increase in Da enhances the streamline intensities thereby assisting downward flow penetration, which causes the streamline lines, i.e., two symmetrical vortices to stretch further away from the top surface. This results in expanding the region for which the convection significantly influences an overall heat transfer process. On the other hand, as the Darcy number decreases, the flow circulations as well as thermal penetration are progressively inhibited due to the

reduced permeability of the medium except at the region close to the location of convection surface condition where the flow motions are relatively strong. Furthermore, figure 5c indicates that as Darcy number approaches zero, the convective heat transfer mechanism is almost suppressed, while the heat transfer by means of conduction plays an important role in heat transfer. The left column of figure 5 shows comparison of temperature in which the contours of different Darcy numbers appear roughly similar.

Figure 6 shows the isotherms and streamlines obtained for various Rayleigh numbers ( $Ra = 10^3, 10^4$  and  $10^5$ ) whereas the Darcy number of 0.1, porosity of 0.8, and h of  $60 \text{ w/m}^2\text{K}$  are fixed. The Rayleigh number provides the ratio of buoyancy forces to change in viscous forces. As Rayleigh number increases, the buoyancy-driven circulations inside the enclosure become stronger as seen from greater magnitudes of stream function. For the large value of Ra ( $Ra = 10^5$ ), there appears a pair of secondary weak circulations in the bottom region of the enclosure. The two vigorous vortices are confined to the upper domain, where convection is a dominant mode of heat transfer.

In what follow, the discussion involves the problem on which convective cooling condition is implemented. The investigations were conducted for a range of controlling parameters, which are Darcy number (Da) Rayleigh number (Ra) and convective heat transfer coefficient (h). The porosity  $\epsilon$  of 0.8 and unity aspect ratio ( $A=1$ ) were considered throughout in the present study. Figure 7 shows the roles of Rayleigh number on heat transfer mechanism/behavior. Various Rayleigh numbers ( $Ra = 5 \times 10^3, 10^4$  and  $5 \times 10^4$ ) whereas the Darcy number of 0.1, porosity of 0.8, and h of  $60 \text{ w/m}^2\text{K}$  are fixed. The Rayleigh number provides the ratio of buoyancy forces to change in viscous forces. As Rayleigh number increases, the buoyancy-driven circulations inside the enclosure become stronger as seen from greater magnitudes of stream function. For large Ra ( $Ra = 5 \times 10^4$ ), contour lines of temperature penetrate faster relative to the low Ra case especially near the central locations. The result is more pronounced for larger Ra. This incident results from strong flow in the downward direction around the central domain. The downward flows assist heat to transfer towards the bottom of the enclosure. In contrast, near the vertical walls where the upward flows are present, the thermal propagation is hindered.

Effects of the Darcy number on the fluid flow and temperature inside the rectangular cavity are depicted in figure 8. The contour of isotherms and streamlines are plotted for different Darcy numbers while  $\mathcal{E}$ , Pr and h are kept at 0.8, 1.0 and  $60 \text{ w/m}^2\text{K}$  respectively. Relatively high Ra of  $5 \times 10^4$  is chosen. The Darcy number, which is directly proportional to the permeability of the porous medium, was set to 0.1 and 0.01. The case in which the porous medium is absent corresponds to infinite Darcy number. The presence of a porous medium within rectangular enclosure results in a force opposite to the flow direction which tends to resist the flow which

corresponds to suppress in the thermal currents of the flow as compared to a medium with no porous (infinite Darcy number). It is evident that the increase in Da enhances the streamline intensities thereby assisting downward flow penetration, which causes the streamline lines, i.e., two symmetrical vortices to stretch further away from the top surface. This results in expanding the region for which the convection significantly influences an overall heat transfer process. Further, the evolution results reveal faster rate of vertical temperature distribution than lateral rate. The results are consistent with the thermal behaviors observed in figure 7 for the same reasoning, which confirms how a flow direction impacts the convection heat transfer. On the other hand, as the Darcy number decreases, the flow circulations as well as thermal penetration are progressively suppressed due to the reduced permeability of the medium. Figure 8d (Da = 0.01) indicates that as Darcy number approaches zero, the two circulations confined within the top domain appear very weak. In the remaining area, the fluid is nearly stagnant with very small temperature gradient suggesting that conduction is dominant due to minimal flow activities.

To confirm the observation made, the local values of Nusselt number (Nu) with corresponding thermal and flow behaviors were traced for Ra of  $5 \times 10^4$ . Data are extracted and depicted in figure 9 at  $\tau$  of 0.02, 0.08 and 0.17. Figure 9a represents local Nu at the top open wall of the three dimensionless times. The streamlines and isotherms are illustrated in figure 9b-c at  $\tau = 0.02, 0.08$  and 0.17 respectively. All three lines have similar shape of concave profile. Nu reaches minimum around the central portion and becomes higher away from the central. The reason behind this result is that temperature gradient is high within the proximity of the center location and higher farther away from the middle. However, at  $\tau = 0.02$ , the variation of Nu in the middle domain is small as indicated by the relatively flat profile along the central zone. This is because the circulations are weak thereby minimal effects of flow activity. However, despite the weak vortices, Nu in overall is initially high at  $\tau_1 = 0.02$  because of large temperature gradient at the top boundary then Nu becomes lower at  $\tau_2 = 0.08$ . At  $\tau_3 = 0.17$ , the local values of Nu have increased and become higher than that at  $\tau_2$  as seen from figure 9d that circulations as well as thermal distribution expand throughout the domain causing the bottom wall temperature to decrease.

### 3. Conclusion

Numerical simulations of natural convection flow through a fluid-saturated porous medium in a rectangular cavity due to convection at top surface were performed. Both the heating and cooling configurations are considered. Transient effects of associated controlling parameters were examined. The two-dimensional flow is characterized mainly by two symmetrical eddies that are initiated by the presence of buoyancy effect. The buoyancy effect is associated with the lateral temperature

gradient at locations near the top surface under the condition that the density gradient is positive in the direction of gravitational force. The cooling and heating flow directions are opposite. Cooling flows are much stronger due to greater buoyancy effects, indicating higher overall convection rate. Heat transfer rate is faster around vertical symmetric line relative to the near-wall regions. Large values of Rayleigh number increase streamline intensities, thus enhancing the downward flow penetration. The temperature stratification penetrates deeper toward the bottom wall, and temperature range within the domain is extended. Therefore it enlarges the region where convection mode is significant. Small values of Darcy number hinder the flow circulations. Therefore the heat transfer by convection is considerably suppressed.

### Acknowledgments

Most of this research is financially supported by the Thailand Research Fund (TRF), contract no. MRG4880017.

### References

- [1] T.L. Bergman, F.P. Incropera, and R. Viskanta, Correlation of Mixed Layers Growth in Double-Diffusive, Salt-Stratified System Heated from Below, *J. Heat Transfer*, Vol. 108, (1986), pp. 206-211.
- [2] J. Imberger and P.F. Hamblin, Dynamics of Lakes, Reservoirs, and Cooling Ponds, *A. Rev. Fluid Mech.*, Vol. 14, (1982), pp. 153-187.
- [3] M.A. Stanish, G.S. Schager, and F. Kayihan, A Mathematical Model of Drying for Hygroscopic Porous Media, *AIChE J.*, Vol. 32, (1986), pp. 1301-1311.
- [4] P. Ratanadecho, K. Aoki, and M. Akahori, A Numerical and Experimental Investigation of the Modeling of Microwave Drying Using a Rectangular Wave Guide, *J. of Drying Tech.*, Vol. 19(9), (2001), pp. 2209-2234.
- [5] P. Ratanadecho, K. Aoki, and M. Akahori, Influence of Irradiation Time, Particle Sizes and Initial Moisture Content During Microwave Drying of Multi-Layered Capillary Porous Materials, *ASME J. Heat Transfer*, Vol. 124 (1), (2002), pp. 151-161.
- [6] P. Cheng, Heat transfer in geothermal systems, *Advances in Heat Transfer*, Vol. 4, (1978), pp. 1-105.
- [7] P.H. Oosthuizen and H. Patrick, Natural Convection in an Inclined Square Enclosure Partly Filled with a Porous Medium and with a Partially Heated Wall, *American Society of Mechanical Engineers, Heat Transfer Division*, (Publication) HTD 302, (1995), pp. 29-42.
- [8] P. Nithiarasu, K.N. Seetharamu and T. Sundararajan, Natural Convective Heat transfer in a Fluid Saturated Variable Porosity Medium, *International Journal of Heat and Mass Transfer* 40 (16), (1997), pp. 3955-3967.
- [9] K.M. Khanafer and A.J. Chamkha, Mixed

Convection Flow in a Lid-Driven Enclosure Filled with a Fluid-Saturated Porous Medium, International Journal of Heat and Mass Transfer 42 (13), (1998), pp. 2465-2481.

- [10] P. Nithiarasu, K.N. Seetharamu and T. Sundararajan, Numerical Investigation of Buoyancy Driven Flow in a Fluid Saturated non-Darcian Porous Medium, International Journal of Heat and Mass Transfer 42 (7), (1998), pp. 1205-1215.
- [11] P. Bera and A. Khalili Double-diffusive natural convection in an anisotropic porous cavity with opposing buoyancy forces: multi-solutions and oscillations, Int. J. Heat Mass Transfer, Vol. 45, (2002), pp. 3205-3222.
- [12] P. Bera, V. Eswaran, P. Singh, Numerical study of heat and mass transfer in an anisotropic porous enclosure due to constant heating and cooling, Numer. Heat Transfer, Part A, Vol. 34, (1998), pp. 887-905.
- [13] H.C. Brinkmann, On the permeability of media consisting of closely packed porous particles, Appl. Sci. Res., Vol. 1, (1947), pp. 81-86.
- [14] G. Lauriat and V. Prasad, Natural convection in a vertical porous cavity: a numerical study for Brinkmann-extended Darcy formulation, Trans. ASME J. Heat Transfer , Vol. 109, (1987), pp. 295-320.
- [15] A.M. Al-Amiri, Analysis of Momentum and Energy Transfer in a Lid-Driven Cavity Filled with a Porous Medium, Int. J. Heat Mass Transfer, Vol. 43, (2000), pp. 3513-3527.

Figure 1. Schematic representation of the computational domain.

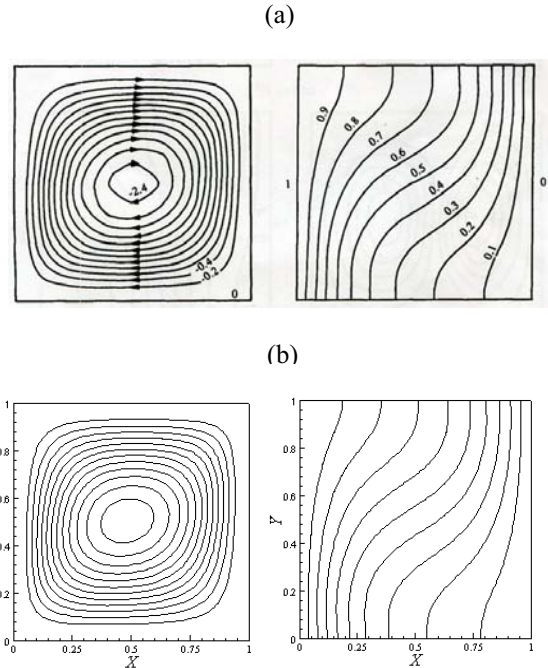


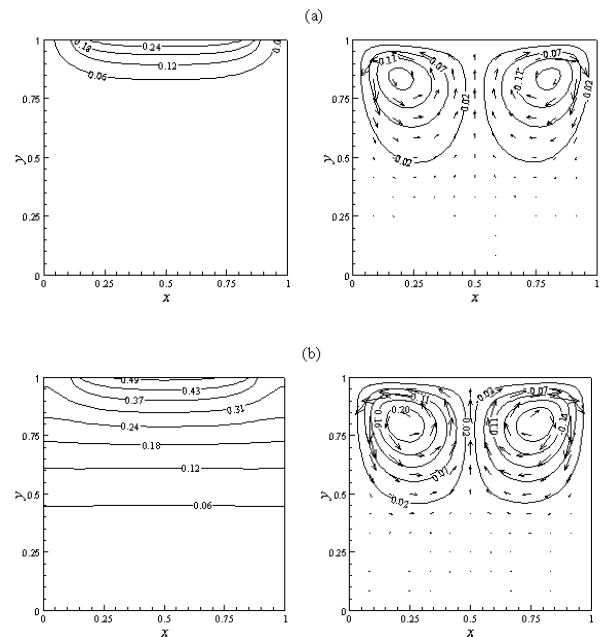
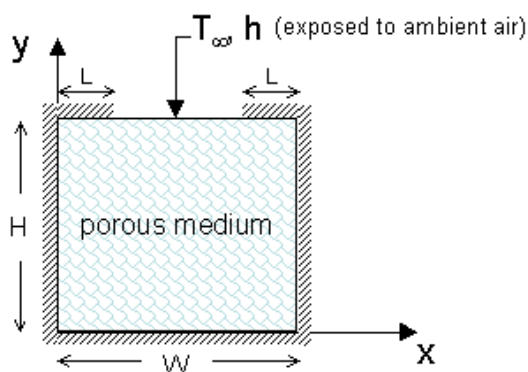
Figure 2. Test results for validation purpose: a) Nithiarasu et al. [8]: Non-Darcian model (including inertial and boundary effect) b) present simulation: Brinkman-extended Darcy model, which accounts for viscous effects.

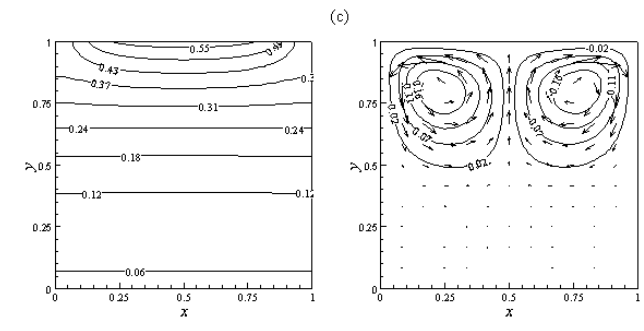
Table

Table 1. Comparison of the results obtained in the present study with those of Nithiarasu et al. [8] (Da=0.01, Ra = 10<sup>3</sup>, porosity = 0.6)

	Present work	Published work [8]	Difference (%)
$\psi_{max}$	2.53	2.56	1.17
$V_{max}$	9.49	9.34	1.60

Figure





contours of temperature and streamlines at times  $\tau =$  (a) 0.013, (b) 0.088, (c) 0.168, and (d) 0.245. ( $Ra = 5 \times 10^4$ ,  $Da = 0.1$ ,  $Pr = 1.0$ ,  $\varepsilon = 0.8$ , and  $h = 60 \text{ W/m}^2\text{K}$ )

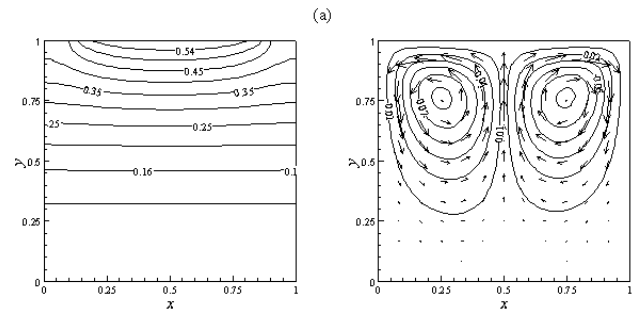


Figure 3. Sequential files with the heating boundary for contours of temperature and streamlines at times  $\tau =$  (a) 0.013, (b) 0.088, and (c) 0.168. ( $Ra = 5 \times 10^4$ ,  $Da = 0.1$ ,  $Pr = 1.0$ ,  $\varepsilon = 0.8$ , and  $h = 60 \text{ W/m}^2\text{K}$ )

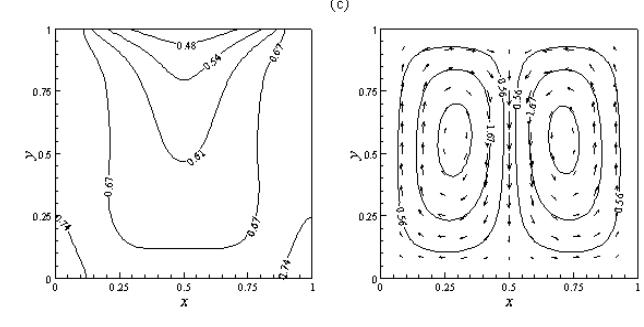
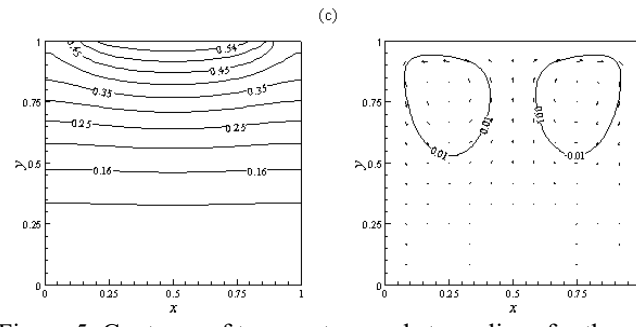
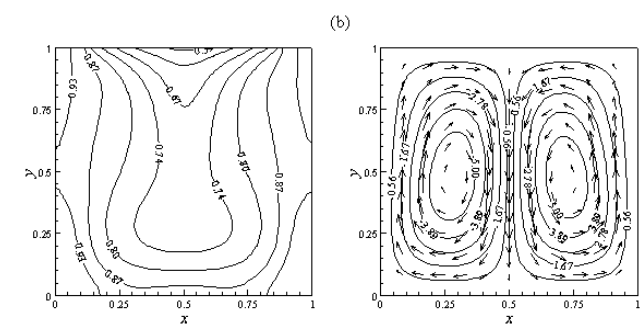
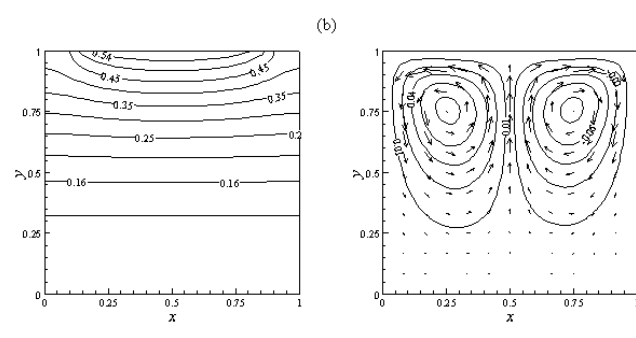
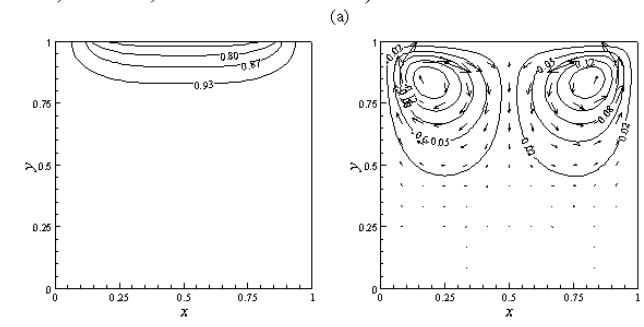


Figure 5. Contours of temperature and streamlines for the heating case (a)  $Da = \text{infinity}$  (b)  $Da = 0.1$  (c)  $Da = .001$ . ( $Ra = 10^4$ ,  $h = 60 \text{ W/m}^2\text{K}$ ,  $Pr = 1.0$ , and  $\varepsilon = 0.8$ )

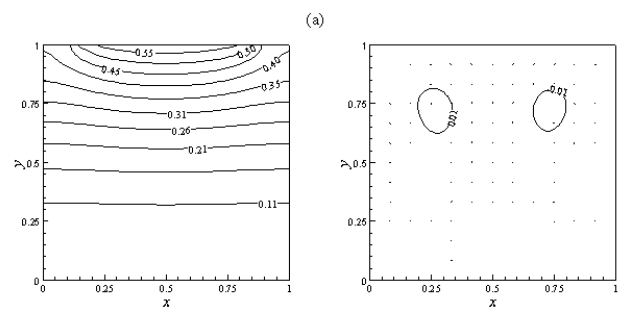
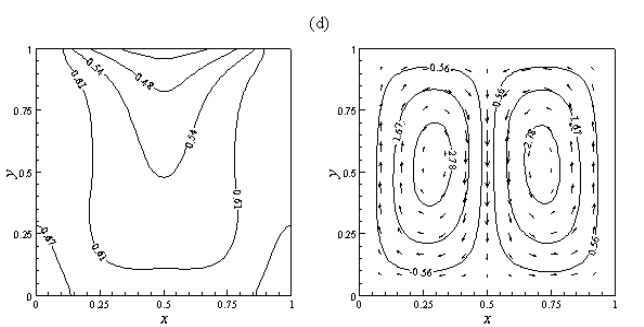


Figure 4. Sequential files with the cooling boundary for contours of temperature and streamlines at times  $\tau =$  (a) 0.013, (b) 0.088, and (c) 0.168. ( $Ra = 5 \times 10^4$ ,  $Da = 0.1$ ,  $Pr = 1.0$ ,  $\varepsilon = 0.8$ , and  $h = 60 \text{ W/m}^2\text{K}$ )

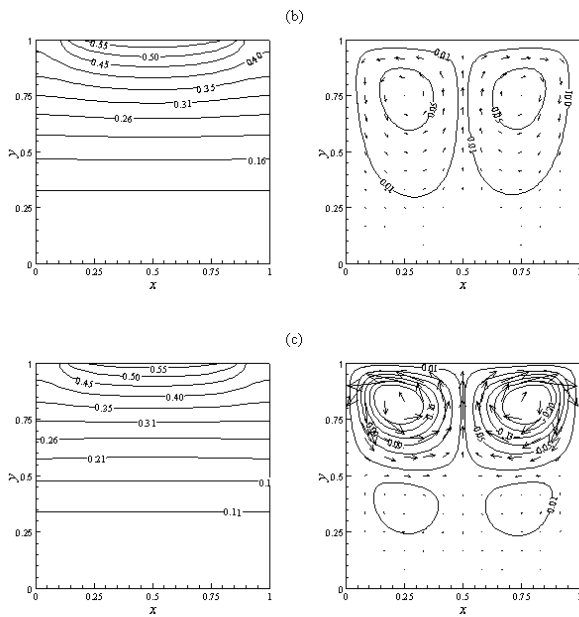


Figure 6. Contours of temperature and streamlines for the heating case (a)  $Ra = 10^3$  (b)  $Ra = 10^4$  (c)  $Ra = 10^5$ . ( $Da = 0.1$ ,  $h = 60 \text{ W/m}^2\text{K}$ ,  $Pr = 1.0$ , and  $\varepsilon = 0.8$ )

Figure 7. Contours of temperature and streamlines for the cooling case (a)  $Ra = 5 \times 10^3$  (b)  $Ra = 10^4$  (c)  $Ra = 5 \times 10^4$ . ( $Da = 0.1$ ,  $h = 60 \text{ W/m}^2\text{K}$ ,  $Pr = 1.0$ , and  $\varepsilon = 0.8$ )

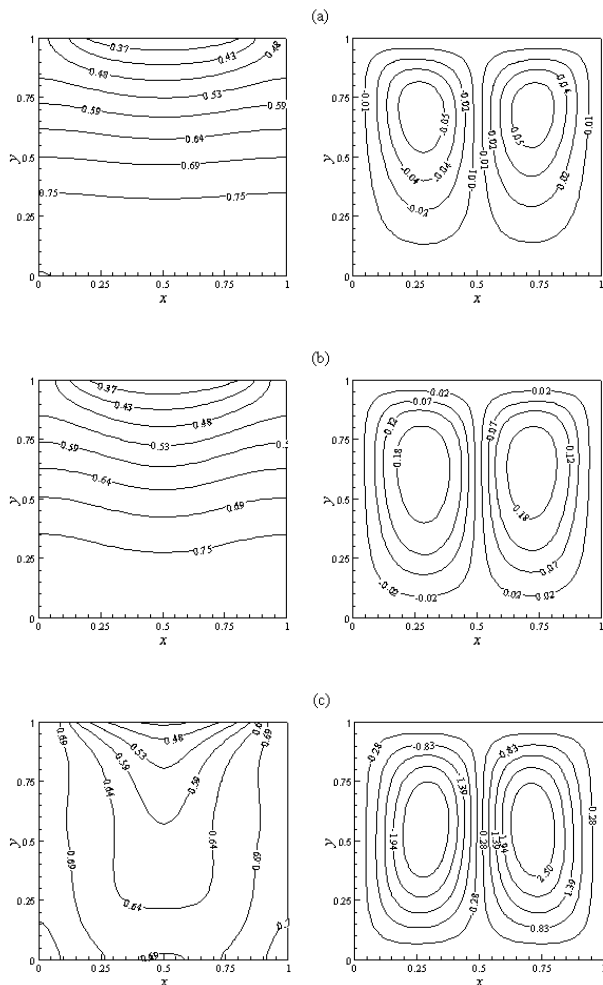
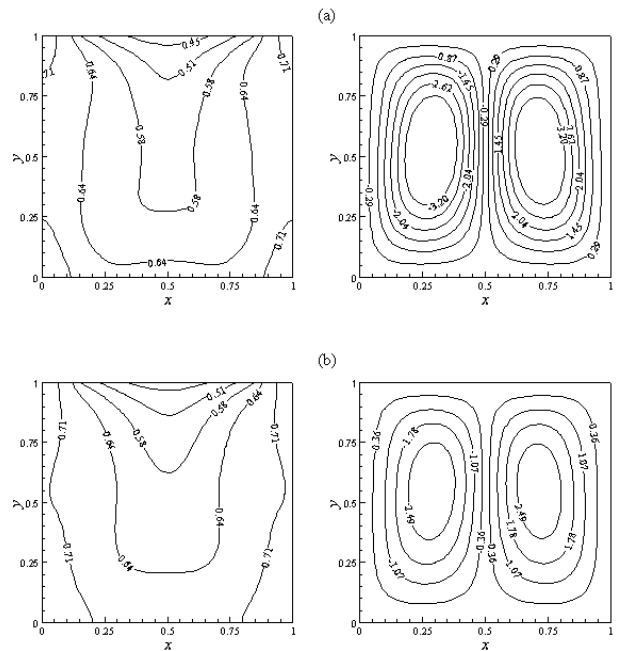


Figure 8. Contours of temperature and streamlines for the cooling case (a)  $Da = \text{infinity}$  (b)  $Da = 0.1$  (c)  $Da = .001$ . ( $Ra = 5 \times 10^4$ ,  $h = 60 \text{ W/m}^2\text{K}$ ,  $Pr = 1.0$ , and  $\varepsilon = 0.8$ )

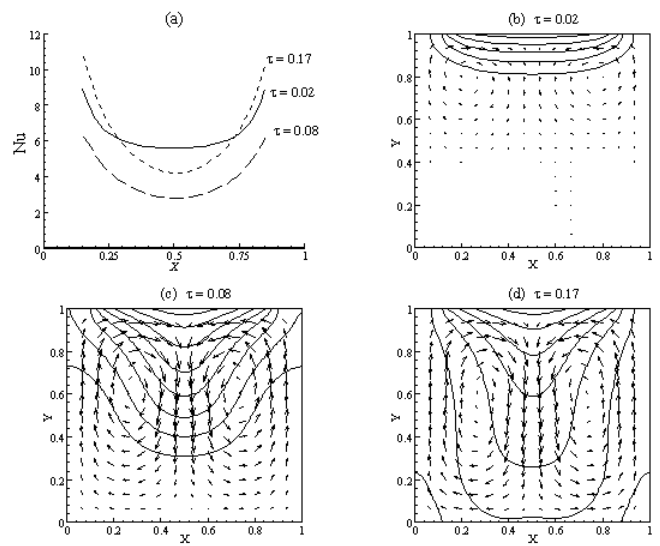


Figure 9. Local Nusselt numbers at three different times.